Journal of
Materials Sciences and Applications

JScholar
Fostering Scholarly Communication

Research Article Open Access

Heat Capacities $C_p(T)$ of the Isostructural Sphalerite Phases as a Single System in Solid State

Vassiliev Valery P*

Chemical Department, Lomonosov Moscow State University, Moscow 119991, Russia

***Corresponding author:** Vassiliev V, Chemical Department, Lomonosov Moscow State University, Moscow 119991, Russia, Tel: +74954415412, Email: valeryvassiliev@yahoo.fr

Received Date: May 04, 2022 **Accepted Date:** May 31, 2022 **Published Date:** Jun 02, 2022

Citation: Vassiliev V (2022) Heat Capacities Cp(T) of the Isostructural Sphalerite Phases as a Single System in Solid State. J Mater sci Appl 6: 1-16

Abstract

The standard thermodynamic constants are important for all branches of science. The correct description of heat capacities in a wide range of temperatures is to find a rigorous description to this still unsolved problem. A fragmental description of some phases is like a vision of one part of a large mosaic picture. A single description of the heat capacity or other property of a phase of any isostructural series does not allow one to see the integrity of the entire ensemble. The nontrivial concept permitted us the possibility of finding a simple solution to this issue. This solution helped describe the specific heat in a wide temperature range of a large class of isostructural sphalerite phases as a single system unambiguously. The 4th group of pure elements as silicon, germanium, alpha tin, and diamond-like lead was taken as the base. Flerovium (^{114}Fl) closes this group. There should be no other elements in this group according to the fine structure constant (α) or the Sommerfeld constant. As a consequence, the limiting value of the heat capacities of phases with a sphalerite structure falls on the 114th element (^{114}Fl) and has a value of C_p = 30.5±0.3 J · mol-at^{-1} · K^{-1}. This value was obtained as a maximal virtual point C_p of the last elements (^{114}Fl) of the IV group and corresponds to Ln (C_p / R) = 1.30±0.01 for the isotherms Ln (C_p / R) vs Ln (N), where N is an atomic number of an element of the IV group or the sum of the atomic numbers of $A^{III}B^{V}$ or $A^{II}B^{VI}$ compounds per mole-atom. The common point of heat capacity attributable to flerovium is obtained from the linear equations C_p/R vs Ln(N) at low temperatures from 25 to 35K. If we consider only pure elements of the 4th group: silicon, germanium and alpha-tin, then flerovium closes this group, and there are no other elements behind it according to the constant (alpha) of Sommerfeld. The maximum heat capacity of flerovium can be taken as a constant value of 30.5 J·mol-at^{-1}·K^{-1} with an accuracy of 1%. As the temperature decreases, this value slowly decreases (within 1%), and then, when it approaches to 0 K, it drops sharply to 0 J·mol-at^{-1}·K^{-1}. The proposed model was taken as an ideal crystal that does not have any foreign inclusions, defects, or dislocations. Thus, it is quite obvious that other types of heat capacities of structural compounds will have their own maximum values C_p.

Keywords: Fine Structure Constant, Sphalerite Phases, Pure Elements IV Group, Ultimate Value C_p, Similarity Method, Objective Function

Introduction

Thermodynamic analysis of the heat capacity of an individual system, without considering the general class of isostructural compounds, which this system is part of, does not allow one to determine actual behavior C_p vs. temperature. Currently, we have a sufficient set of such data that allow us to carry out a unified comprehensive analysis of the heat capacities.

Let us consider, as an example, the class of optoelectronic materials of diamond-like systems $A^{III}B^{V}$, $A^{II}B^{VI,}$ and the pure elements of the 4th group of the Periodic Table of Elements with a sphalerite structure. The most controversial is the behavior of the heat capacity at low temperatures (below 40K) and high temperatures above 1000K. While the ultimate heat capacity C_v is established by the Dulong and Petit rule [1] with constant 3R, the limiting value of the heat capacity at constant pressure C_p remains unclear until now.

The heat capacity at the constant pressure C_p can be expressed as $C_p = C_v + (\alpha_{t\text{-}ex})^2 BVT + cT$, where the first term is the lattice contribution; the second term is the contribution due to volume change, with B being the bulk modulus, V being the molar volume, and *a* being the volume thermal expansion; the third term is the electron contribution with c known as the electronic constant [2]. The unknown parameters can be measured experimentally or calculated. For example, the calculated coefficients of linear thermal expansion for the wurtzite AlN phase ($\alpha_{t\text{-}ex}$) were obtained in [3]. The difference between C_p and C_v increases for AlN with the increasing of temperature and compounds about 6% at 1200*K*. At a temperature close to T_m = 4840 ±50K, this value can be in the range of 3.7 R to 3.8 R [4], where R=8.31447 mol-at^{-1} K^{-1}. The fourth group of diamond-like elements contains silicon, germanium, alpha tin, and diamond-like lead [5] and flerovium (^{114}Fl) closes this group. There should be no other elements in this group according to the fine structure constant or the Sommerfeld constant $\alpha = e^2 / \hbar c$ [6].

In this expression, e is the electron charge, c is the speed of light, ħ is the reduced Planck's constant, or Dirac's constant ($\hbar = h / 2\pi$). The parameter α is a dimensionless quantity, and its numerical value is close to 1/137. The fine structure constant determines the limit of the maximum number of protons in the nucleus, at which electrons can still have stable orbits. In other words, this constant allows us to determine that with the highest probability, the last neutral atom of the periodic table will be element 137. Researchers [7] share the same opinion.

Discussion about the last element of the Periodic Table remains open. In private correspondence, Academician Y. Oganesyan [8] expressed his personal opinion to me: "It is not at all easy to indicate which element will be the last. Definitely, this is not 119th or 120th. This follows from the properties of elements from 112 to 118, and nuclear stability may end before element 137. Nuclear forces are unknown to us, and predictions here are unfounded. As for the various scenarios for the continuation of the Periodic Table in the field of atomic numbers over 121, this is not my opinion at all but calculated literary data." In the case of diamond-like phases with a sphalerite (zinc blend, *F43m*) structure, the ultimate value of the heat capacity falls on the 114-th element (^{114}Fl) with C_p = 30.5±0.3 J mol-at^{-1} K^{-1} =3.67 R J mol-at^{-1} K^{-1}. This quantity arises when constructing the linear dependencies Ln (C_p/R) *vs* Ln(N) in the temperature region 20-35K. They give us a common point Ln (C_p/R) = 1.3±0.013. This fact permits us to use this point as a reference one.

Materials and Methods

Method

The main idea of this work without details is presented in the shot communication [9].

The functions C_p and C_v using both the Debye models and the Maier-Kelley equation are proposed to describe the heat capacity of substance in a solid state using an in-house software [10], based on the commercial DELPHI-7. The solution to the problem was reduced to finding the minimum of the objective function of eight independent adjustable parameters of the form: $s^2 (T_0, a, b, A_1, Q_1, A_2, Q_2, A_3, Q_3) = \sum_{i=1}^{n}(C_{p,calc} - C_{p,exp})^2/n$ (1)

The search for the minimum of σ^2 was carried out by three methods: the golden ratio, conjugate gradient, and coordinate descent.

They make it possible to calculate the heat capacity values equal to the experimental data within the deviation range.

Materials. Choice of reference elements

What substance can we choose as the standard one? No reference incorporates the influence of impurities on the measurements of the heat capacity of diamond. The heat capacity of diamond has been studied on industrial samples with a content of 0.2 wt. % in [11,12] and up to 1 wt. % of impurities in [13].

Esterman and coworkers [14], studied the effect of alloying additions on the heat capacity of Ge at temperature range 20–200 K. They found the heat capacity of germanium with an aluminum content up to 0.006 at. % gives a significant deviation up to 0.17 J·(mole-atom)$^{-1}$·K^{-1}) in comparison with pure germanium. So, the influence of the impurity on the measure of heat capacities of isostructural diamond and c-BN is quite significant [9]; therefore, it is not possible to take the diamond as a standard substance. Thus, we have chosen the C_p(T) of high-purity Si as a main standard substance up to 700K [15, 16]. We re-optimized C_p(T) data above 700K according to our new concept [10].

The heat capacities of Si and Ge from 0 to 300 K, and virtual point C_p (^{114}Fl) taken as constant were used as main control points. The heat capacities of other diamond-like phases (HgSe and HgTe) with a sphalerite (ZnS) structure served as auxiliary values. Thus, our data on C_p(T) for other phases with a sphalerite structure in the solid state are practically independent of the experimental values. To select the low-temperature heat capacities (C_p) of phases with a sphalerite structure, we used the dependencies Ln (C_p/R) *vs* Ln(N), where N is the number of elements of the Periodic Table (Fig.1). The general expression of a polynomial in the form (2) was used to describe the heat capacities of phases with a sphalerite structure.

$$\text{Ln}\,(C_p/R) = ax^3+bx^2+cx+d+ex^{-1}, \text{ where } x = \text{Ln}(N) \qquad (2)$$

To describe the heat capacities from 15K to 140K, the last three terms of the polynomial were sufficient. The range of the heat capacities from 20K to 35K can be described by a straight-line equation. This gives us the possibility to find the point of intersection in Fig.1 with a precision up to 1% and equal 1.3±0.013. Thus, the uncertainty of extrapolation C_p(T) at high temperatures can be eliminated.

To describe the isotherms of high-temperature heat capacities of diamond-like phases with a sphalerite structure above room temperature, we used as main control points the reoptimized values C_p(Si), C_p(Ge), our experimental C_p(HgTe) [17] and virtual point C_p(^{114}Fl). All curves C_p vs (Ln(N)) are concentrated at one point with coordinates C_p = 30.5±0.3 J mol-at^{-1} K^{-1} and Ln(N) = 4.7362, where N is the atomic number of the 114th element (^{114}Fl). (See Fig.2).

In our recent publication [10], we have shown the enormous influence of impurities and the deviation from stoichiometry chemical compounds on the measured values of the specific heats. Only high-purity elements and strictly stoichiometric compounds can be used for low-temperature heat capacity measurements.

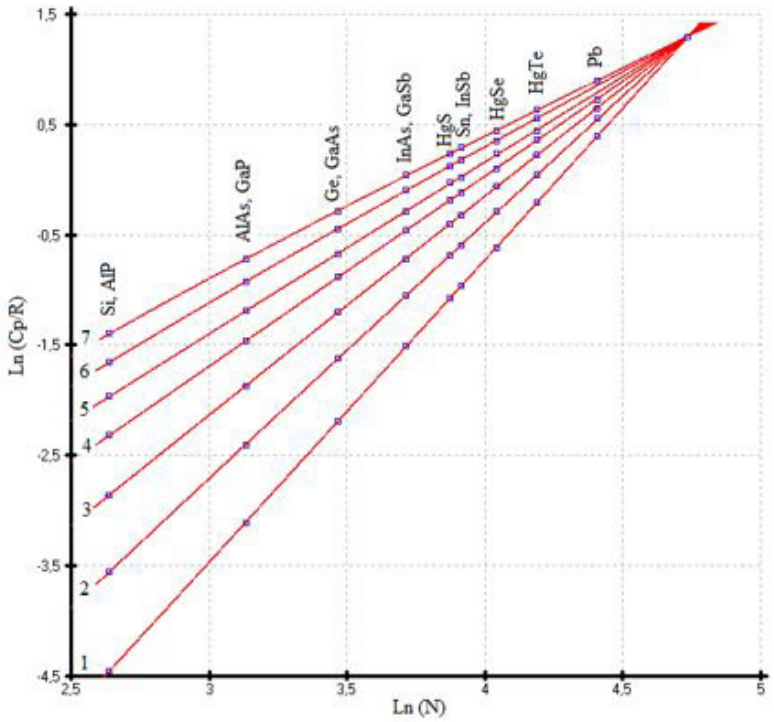

Figure 1: Low temperature isotherms Ln(C_p/R) vs Ln(N) of diamond-like phases with sphalerite structure. 1) 20, 2) 25, 3) 30, 4) 35, 5) 40, 6)45, 7) 50K

It is also convenient to use the form C_p *vs* Ln(N) above 50K

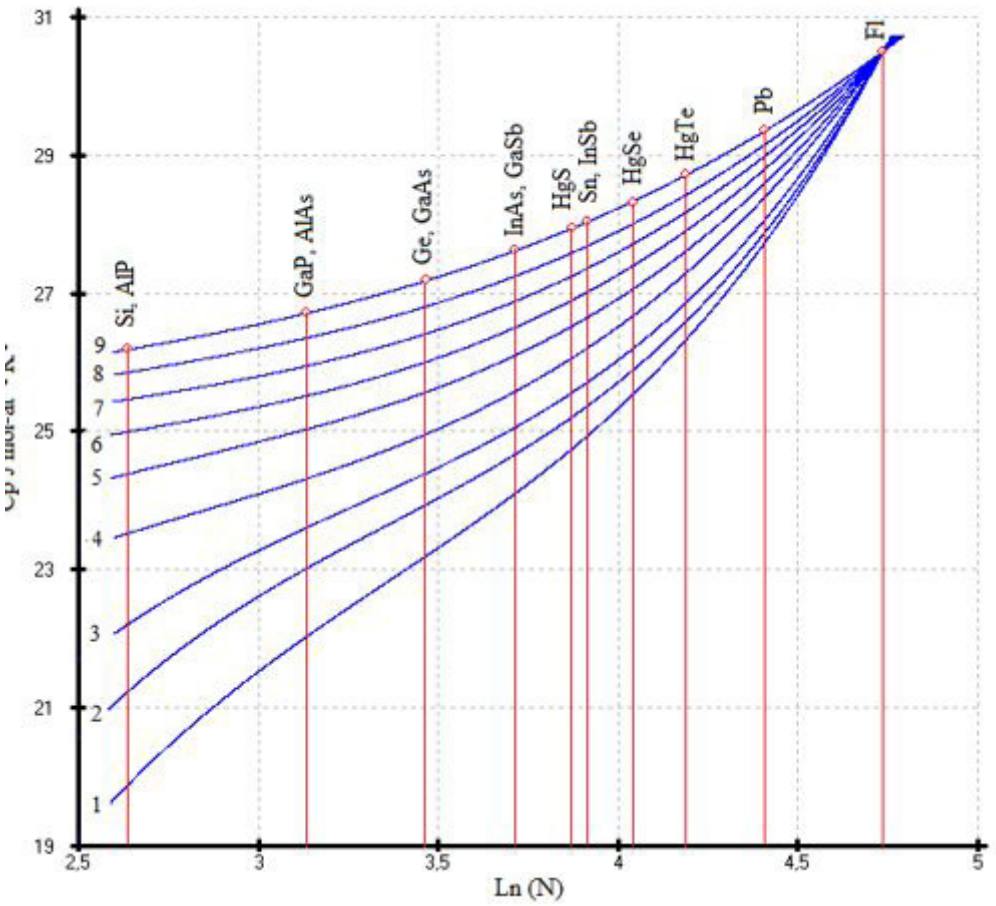

Figure 2: C_p vs Ln(N). Isotherms $C_p = ax^3 + bx^2 + cx + d + ex^{-1}$; (x=Ln(N) of the like-diamond phases 1) 298, 2) 350, 3) 400, 4) 500, 5) 600, 6) 700, 7) 800, 8) 900, 9) 1000K [9]

Results and Discussions

Si and AlP phases

The ensemble of the experimental values $C_p(T)$ of the isostructural phases Si and AlP having the same sum of atomic number per mole-atom was re-optimized. The low-temperature heat capacities were taken from 0 to 300K without any change according to ref [10]. The heat capacities $C_p(T)$ above 300K were re-optimized according to the new concept of a unique point with the coordinate C_p = 30.5±0.3 J mol-at^{-1} K^{-1} and Ln (N) = 4.7362, where N is the atomic number of the 114th element (^{114}Fl), for the set of sphalerite phases. The calculated values of the heat capacities C_p (Si) and C_p (AlP) above 600K were taken from ref. [18,19], respectively, as standard ones. The new proposed conception was not used in our recent article [10]. So, the two alternative descriptions were proposed for the pure silicon and isostructural AlP and Si phases due to the absence of the rigid solution. (See Table 1, equ.1a and 1b). On the one hand, the maximal C_p(Si) at T_m(Si) = 1688±5K [20] gives us the value 29.06 J mol-at^{-1} K^{-1} (equ.1a), and it is suitable for our new concept; on the other hand, the maximal C_p(AlP) at T_m(AlP) = 2800±50K [20] gives us the value 33.023±0.33 J mol-at^{-1} K^{-1} (Table 1, equ.1b), so it is completely unsuitable for this concept. Since we use a single description $C_p(T)$ for two isostructural phases Si and AlP with the same sums of atomic number (N=14) per mole-atom at high temperature, it is reasonable to describe the two phases using the calculated values $C_p(T)$ from ref. [18, 19]. In this case the maximal C_p(AlP) at its T_m gives us the value 30.77±0.31 J mol-at^{-1} K^{-1} (Table 1, equ.1c). So, we can accept the equation 1c, Table 5 as standard above the room temperature for the Si and AlP phases. Some additional increases in the heat capacity of silicon at elevated temperatures can be explained by the oxidation of its surface. Under normal atmospheric conditions, a thin (1-2 nm) layer of silicon dioxide forms on the silicon surface. Its layer grows upon heating, up to tens of nanometers [22]. The description of the heat capacities of Si and AlP phases was done by a multiparameter family of functions [10]. We use all previous references from [10], except the data [15] above 700K (See Fig.3 (this work), and Tables 5-8 [10]).

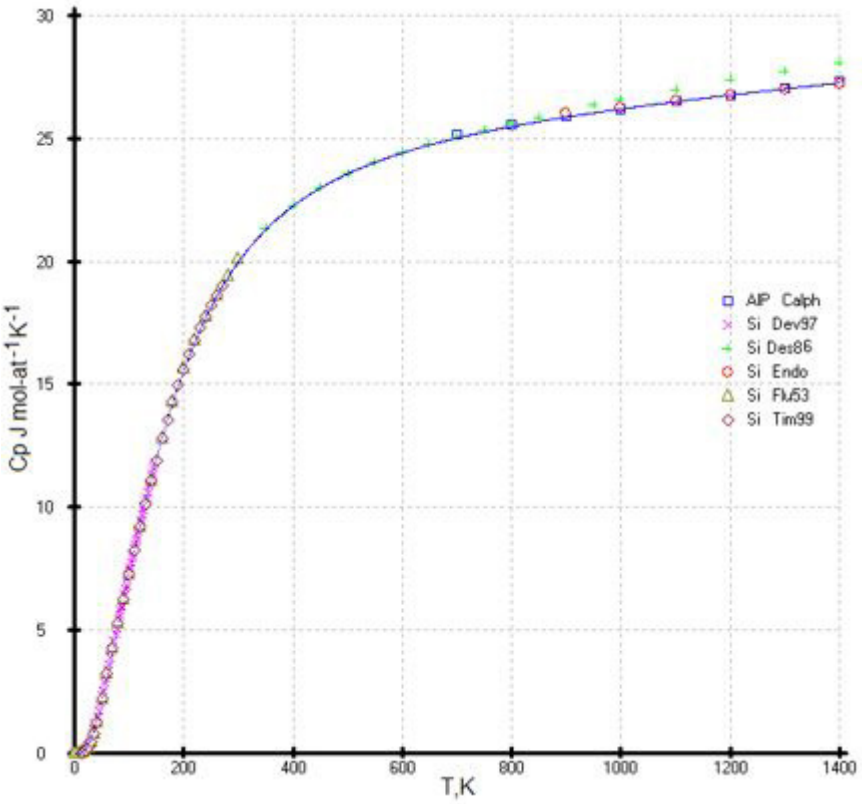

Figure 3: Re-optimized description of the heat capacities of Si and AlP using a combination of this model and multiparameter family of functions [10]. Experimental points: ○[18], □[19], +[21], x[15], Δ[23], ◊[16], The points + [21] were used only in the range 298 - 700K

Table 1: Parameters of Maier-Kelley equations C_p^{MK} = a + b10^{-3}T - c10^{5}T^{-2} (J·(mole-atom)$^{-1}$·K^{-1}) at the high temperature region

No	Phase	a	b	c	T. K range	n	σ^{MK}	Reference
1a	Si	23.55	3.394	4.138	300-1500	31	0.04	[10]
1b	Si, AlP	23.34	3.476	3.837	300-1500	66	0.23	[10]
1c	Si, AlP	24.31	2.319	4.550	300-1500	31	0.08	This work
2	GaP, (AlAs)	23.53	3.369	2.182	300-1000	9	0.02	This work
3a	Ge	23.45	3.740	1.162	324- 753	29	0.05	[10]
3b	Ge, (GaAs)	23.45	3.813	1.185	300-1500	28	0.05	This work
4	InAs, GaSb	24.43	3.339	1.192	300-1000	9	0.02	This work
5a	α-Sn, (InSb)	25.25	2.958	1.121	300-1000	9	0.01	This work
5b	α-Sn, InSb	24.32	4.723	0.1776	800-1000	6	0.07	[10]
6	HgS	24.98	3.036	1.062	300-1000	12	0.02	This work
7	HgSe	25.88	2.506	1.061	300-1000	12	0.04	This work
8	HgTe	26.14	2.944	0.4395	300-1000	12	0.02	This work
9	Pb	27.25	2.414	0.3818	300-1000	12	0.02	This work

Table 2: Parameters of function (1) in the range 0.1 - T_m K

No	Phase	n	T_o	A_1	Θ_1	A_2	Θ_2	A_3	Θ_2	a	b	$\sigma 10^2$
1	Si. AlP	77	230	0.350	338.8	0.365	819.1	0.285	852.6	24.31	2.319	6
2	Ge	137	313.7	0.358	187.7	0.330	467.2	0.311	504.2	23.45	3.813	11
3	α-Sn	27	82.5	0.464	128.3	0.227	338.7	0.309	380.1	25.25	2.958	6
4	AlAs GaP	33	429.9	0.484	281.1	0.210	693.1	0.305	714.7	23.53	3.369	7
5	InAs GaSb	31	299.6	0.435	160.9	0.260	417.5	0.306	429	24.53	3.369	10
6	HgS	27	64.9	0.451	133.3	0.242	356.1	0.307	380.1	24.96	3.060	7
7	HgSe	27	220.8	0.428	98	0.267	272.7	0.305	315.4	25.88	2.506	8
8	HgTe	27	52.7	0.523	83.7	0.204	265.8	0.273	287.3	26.32	2.401	7
9	Pb	26	36.6	0.396	74.2	0.396	74.5	0.208	300.9	27.25	2.414	14

Ge and GaAs phases

The heat capacities of Ge and GaAs served as a second main control point. The description $C_p(T)$ for the Ge phase gave us the same values as in ref. [10] and did not differ from previous values (Table 5, 3a) despite the minimal difference of the coefficients. The description of the heat capacities of Ge by a multiparameter family of functions is presented in [10].

GaP and AlAs phases

The heat capacities $C_p(T)$ of GaP and the unstudied isostructural GaAs phases can be obtained by interpolation between the two control values of $C_p(T)$ for the pure Si and Ge phases. The calculated $C_p(T)$ for GaP were also treated by a multiparameter family of functions [10] (solid line in Fig.4) and compared with the superposed experimental points. This comparison shows the good concordance for the temperature above 70K. The disaccord between our model and the experimental values $C_p(T)$ in region 15-70K we attribute to the deviation of the composition of the measured sample from stoichiometry and the presence of the impurities, which leads to an increase of the heat capacity and entropy in the considered temperature region. Our calculated heat capacities were obtained by interpolating linear or quasi-linear equations of the form Ln (C_p / R) vs Ln(N) between two well-studied standard pure elements: silicon and germanium (See Tables 3and 4). The curve $C_p(T)$ for GaP calculated using our model is presented in Fig.4. The experimental points were superposed after the calculation.

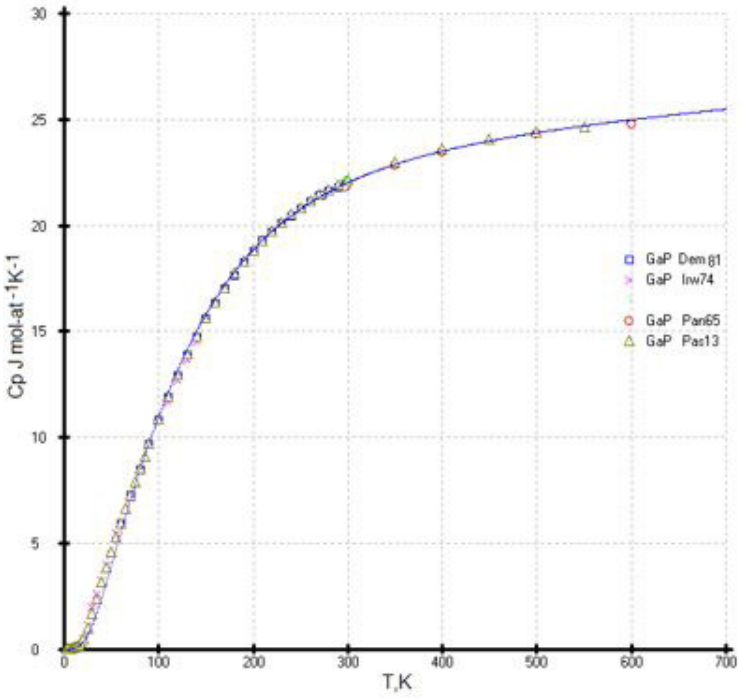

Figure 4: The independent curve Cp(T) for GaP calculated using a combination of this model and multiparameter family of functions [10]. The experimental points: ❑[30], x[29], ○[31], Δ[32] were superposed after the calculation

Table 3: The recommended $C_p(T)$ of like-diamond phases at low temperature in $(J\cdot(mol\text{-}at)^{-1}\cdot K^{-1})$

Phase T, K	Si, AlP [10]	AlAs, GaP	Ge, GaAs [10]	InAs, GaSb	Sn, InSb	HgS	HgSe	HgTe	Pb
5	0.00048	0.0018	0.0050	0.015	0.044	0.0365	0.10	0.269	0.300
10	0.00596	0.021	0.0667	0.213	0.450	0.4029	0.90	1.699	3.311
15	0.0300	0.117	0.330	0.711	1.432	1.255	2.53	4.100	7.544
20	0.0971	0.366	0.828	1.578	2.871	2.581	4.43	6.624	11.16
25	0.2383	0.707	1.528	2.711	4.443	4.075	6.21	8.625	13.83
30	0.4790	1.187	2.398	3.952	5.957	5.543	7.79	10.37	15.80
35	0.8199	1.790	3.359	5.193	7.356	6.914	9.23	11.86	17.31
40	1.165	2.484	4.348	6.385	8.445	8.180	10.54	13.2	18.51
45	1.589	3.234	5.327	7.511	9.842	9.358	11.77	14.42	19.50
50	2.061	4.010	6.277	8.573	10.97	10.46	12.91	15.52	20.34
55	2.567	4.791	7.190	9.578	12.00	11.49	13.96	16.53	21.07
60	3.095	5.563	8.067	10.53	12.97	12.45	14.92	17.44	21.70
65	3.635	6.319	8.908	11.42	13.88	13.35	15.80	18.26	22.25
70	4.180	7.054	9.715	12.27	14.72	14.19	16.61	19.00	22.74
75	4.725	7.766	10.48	13.07	15.49	14.98	17.33	19.66	23.17
80	5.266	8.456	11.22	13.82	16.21	15.70	17.99	20.25	23.56
85	5.802	9.122	11.93	14.52	16.86	16.37	18.59	20.78	23.90
90	6.331	9.766	12.60	15.18	17.46	16.98	19.13	21.26	24.20
95	6.852	10.39	13.23	15.80	18.02	17.55	19.62	21.68	24.47
100	7.366	10.85	13.84	17.40	18.53	18.08	20.07	22.07	24.72
110	8.369	12.02	15.07	17.04	19.43	19.00	20.84	22.73	25.14
120	9.338	13.04	15.90	18.29	20.20	19.79	21.49	23.27	25.48
130	10.269	13.98	17.00	19.07	20.85	20.46	22.03	23.72	25.77
140	11.161	14.84	17.90	19.74	21.41	21.03	22.49	24.09	26.01
150	12.010	15.63	18.50	20.32	21.89	21.52	22.89	24.41	26.21
160	12.817	16.36	19.12	20.83	22.31	21.95	23.23	24.68	26.39
170	13.579	17.02	19.67	21.28	22.67	22.33	23.53	24.92	26.54
180	14.297	17.63	20.16	21.67	22.99	22.65	23.79	25.12	26.68
190	14.973	18.19	20.59	22.01	23.27	22.94	24.03	25.3	26.80
200	15.606	18.69	20.97	22.32	23.52	23.20	24.23	25.46	26.91
220	16.753	19.58	21.62	22.85	23.94	23.63	24.59	25.72	27.09
240	17.753	20.33	22.15	23.27	24.23	23.99	24.86	25.94	27.24
260	18.625	20.95	22.58	23.62	24.58	24.28	25.13	26.12	27.37
280	19.390	21.49	22.94	23.92	24.78	24.53	25.35	26.28	27.49

Table 4: The recommended $C_p(T)$ of like-diamond phases at high temperature in $(J\cdot(mole\text{-}at)^{-1}\cdot K^{-1})$

T, K	Si, AlP	GaP, AlAs	Ge, GaAs	GaSb, InAs	Sn, InSb	HgS	HgSe	HgTe	Pb sphalerite
298.15	19.90	21.99	23.22	24.15	24.92	24.73	25.52	26.40	27.58
350	21.25	22.88	23.90	24.68	25.37	25.19	25.92	26.70	27.81
400	22.22	23.51	24.40	25.07	25.72	25.53	26.22	26.92	28.00
450	22.96	23.99	24.76	25.38	26.02	25.82	26.47	27.12	28.16
500	23.53	24.37	25.05	25.66	26.28	26.07	26.69	27.29	28.31
600	24.39	24.99	25.57	26.13	26.74	26.50	27.07	27.60	28.60
700	25.00	25.49	26.01	26.54	27.16	26.88	27.40	27.88	28.87
800	25.47	25.93	26.42	26.93	27.55	27.23	27.70	28.15	29.12
900	25.86	26.34	26.81	27.30	27.93	27.57	27.99	28.41	29.38
1000	26.19	26.72	27.19	27.65	28.30	27.90	28.27	28.66	29.63
1100	26.49	27.10	27.53	28.01	28.66	28.22	28.54		
1200	26.76	27.47	27.94	28.36					
1300	27.02	27.83	28.31	28.70					
1400	27.26	28.19	28.68	29.04					
1500	27.49	28.55	29.04	29.38					

GaSb and InAs phases

The description of the heat capacities of the GaSb and InAs phases by a multiparameter family of functions [10] and our model in the range 0-800K is presented in Fig.5. The experimental points were superposed after the description of the calculation. The data [24] for InAs at low temperature and [33] for GaSb phases fit best with our independent description. The data [33-35] are not suitable above 380K and data [24] for GaSb between 90 and 273K, is slightly above our description. We also attribute this error to the deviation of the composition of the measured sample from stoichiometry and the presence of the impurities. The chemically aggressive elements As and Sb and high partial pressure of these at high temperature also affect measurements.

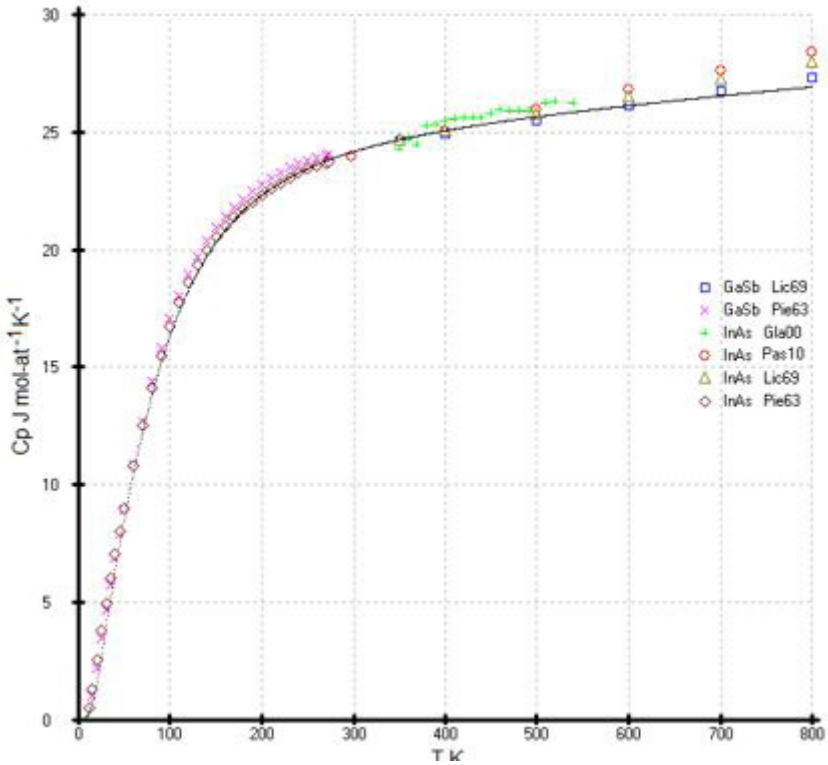

Figure 5: The independent description of the heat capacities of the GaSb and InAs phases by a combination of this model and multiparameter function [10]. Experimental points: ❐[33], x[24], +[34], +[35], ○[33], ◊[24] were superposed after description

Gray tin (α-Sn) phase

The investigation of the heat capacity of gray tin (α-Sn) is difficult due to the kinetic features of the transformation of the white tin (β-Sn) into gray tin (-Sn) and the presence of impurities of other elements. Most of the data on the heat capacity of gray tin were obtained in the first half of the twentieth century [36-38] and compiled in the Hultgren handbook [39].

During the process of the β → α phase transformation of the Sn samples subjected to prolonged exposure at low temperatures, insufficient nucleation was found, which are impurities of other elements, and additional nucleation was required at the kinetically optimal temperature of -45°C (228K). The β → α transformation can be separated into two processes—nucleation and growth. The two processes occur at different rates, and nucleation is the critical event for tin pest formation. Nucleation is associated with long and uncertain incubation periods. Tin can spend anywhere from months to years in cold storage before developing observable signs of tin pest. Following nucleation, growth is relatively rapid, with 100% transformation to α-tin observed to occur in as little as 30 days [40].

The phase transformation of β-Sn ($I4_1/amd$, (tetragonal cell with a = 0.5831 nm, c =0.318 nm) into α-Sn (Fd3m, cubic cell with a = 0.6489 nm) below 286.4K has specific features. Heat capacity measurements β-Sn phase (99.998%) in the range 80-373K showed that this phase remains unchanged [41]. Unfortunately, the heat capacity measurements were interrupted at 80K due to a technical problem.

The impurities and closest crystal-chemical analogues of α-Sn, as InSb (F43m, a = 0.6478 nm) or CdTe (F43m, a = 0.641 nm), help transform β-Sn into α-Sn [42]. The phase transformation of β-Sn (99.9999%) to α-Sn can also occur in ice. In this case, α-Sn is formed when β-Sn comes into contact with the ice crystals in a closed system [43].

Measurements of the low-temperature heat capacity of a-Sn with a purity of less than 99.99%, or if there is an incomplete transformation of β-Sn to α-Sn, can give overestimated $C_p(T)$ values.

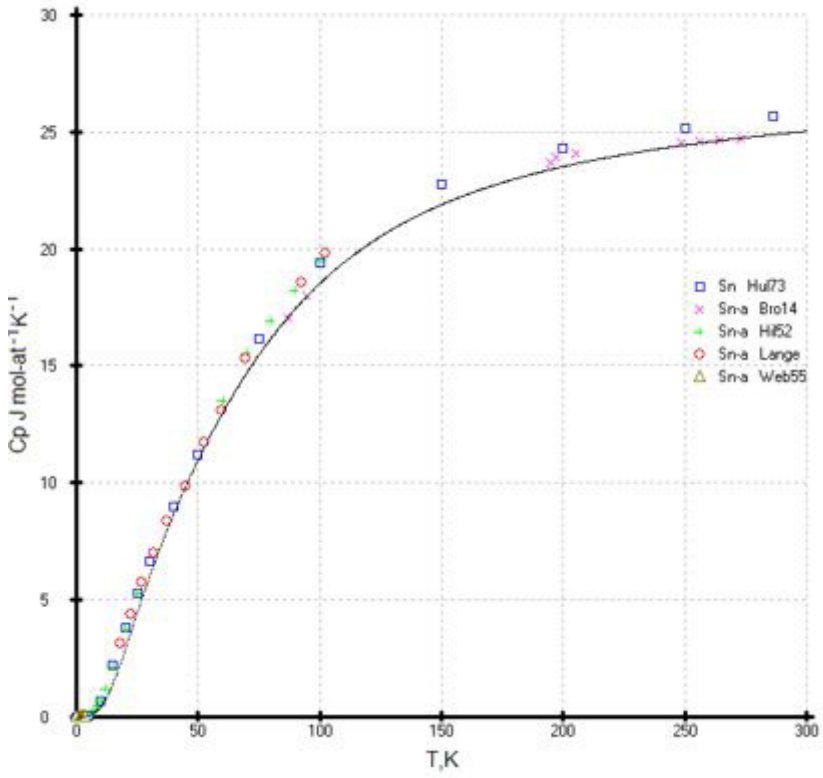

Figure 6: The independent optimized description of the heat capacities of the α-Sn phase using a combination of this model and multiparameter family of functions [10]. The experimental points: x[36], +[25], ○[38], Δ[37], and complied data ❐[39] were superposed after re-optimized description.

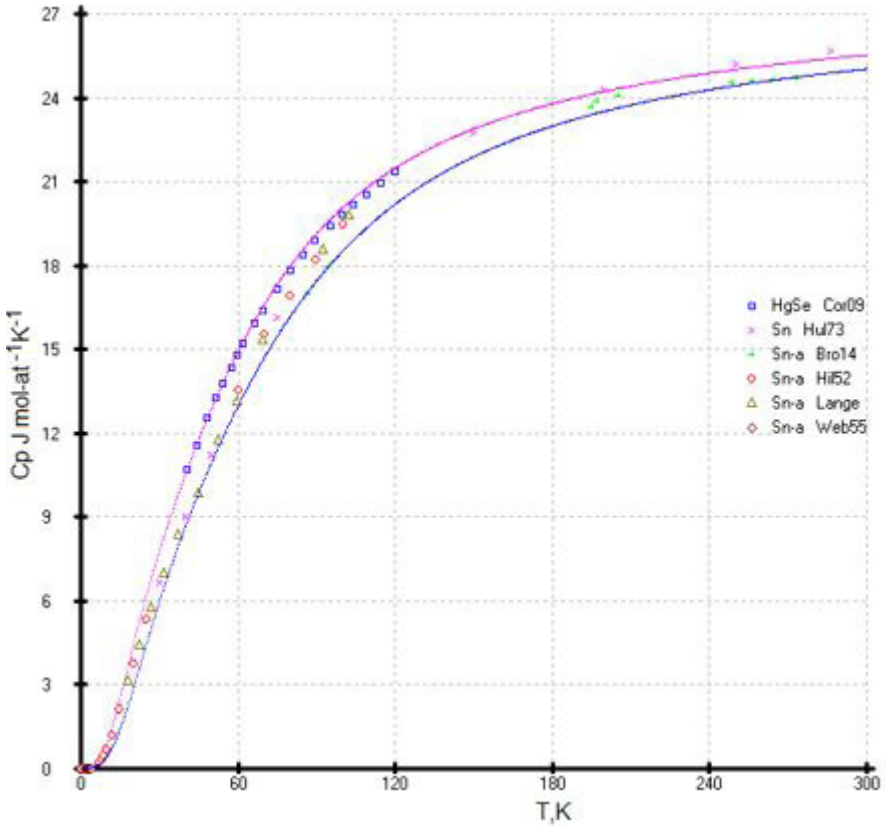

Figure 7: Comparison of two descriptions of the heat capacities of the α-Sn phase (blue line) and HgSe (rad line) using a combination of this model and multiparameter family of functions [10] in the range 0-300K. The all experimental points: Δ[44], x[39], +[36], Δ[25], Δ[38] and ◊[37] were superposed after descriptions. Notes: The descriptions of (α-Sn) and (HgSe) (blue and red) curves were accomplished independently from the experiment points.

Here it is appropriate to compare the experimental heat capacities of α-Sn and its isostructural selenide HgSe [44] (See Fig.7). Unfortunately, the experimental data [44] are presented in a small-sized figure; nevertheless, after their digitization, we were able to analyze the results of the heat capacity of two isostructural phases. The experimental points of the heat capacity of α-Sn tend to move above 60 K to the heat capacity of HgSe, and at temperatures of 140–270 K, according to the compilation [39], they are in complete agreement with the measurements of C_p α-Sn, which completely contradicts the behavior of the heat capacities of the two isostructural phases. Heat capacity data was obtained by the well-known Cordona group and co-workers [44] and is considered reliable. The low-temperature data α-Sn were located between the two heat capacity curves α-Sn and HgSe. The optimized heat capacity of α-Sn is only slightly less than the accepted one in [10].

HgTe phase

The $C_p(T)$ of the HgTe phase at high temperature was calculated using our previous results [17] and literature data [46]. The low temperature heat capacities of the HgTe phase used the corresponding equations of the isotherms $Ln(C_p/R)$ vs Ln(N) (See Tables 3 and 4).

The data [47] has an unexpected comportment above 100K (Fig.8). The curve is not regular in comparison with the recent data [44]. The $C_p(T)$ data [44] were determined by digitizing the figure from this paper in the absence of tabular data. The data proposed in the handbook [31] are above that identified in experimental [11, 46] and our calculated data, and they fall on the calculated curve of diamond-like lead.

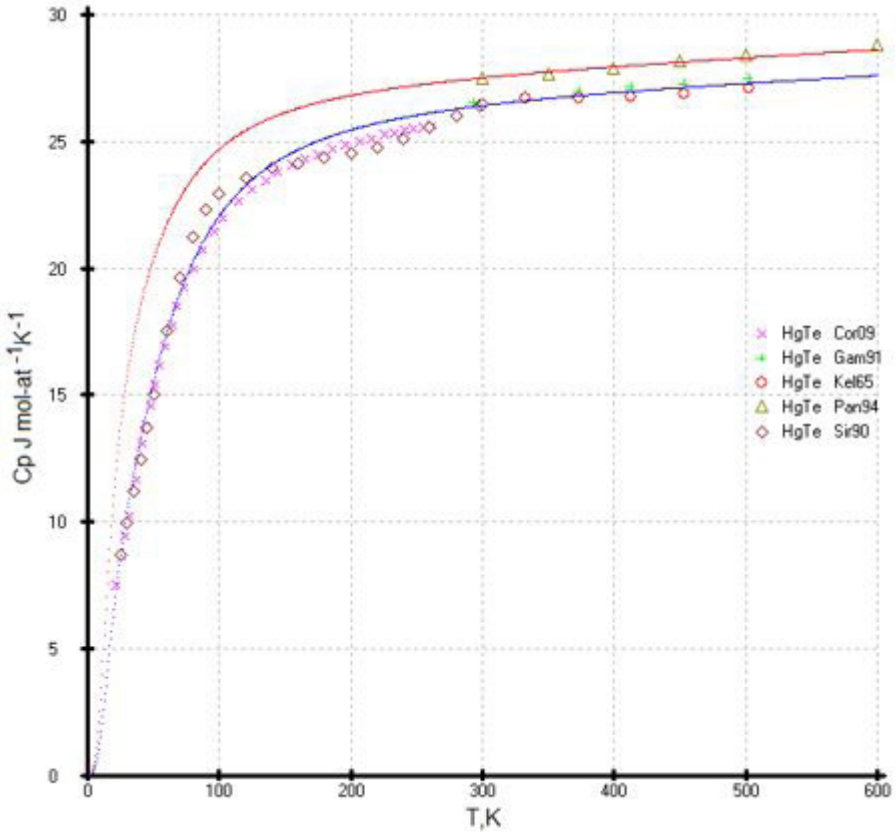

Figure 8: Comparison of two descriptions of heat capacities of the HgTe phase (blue line) and diamond like Pb (rad line) using a combination of this model and multiparameter family of functions [10] in the range 0-600K. The all experimental points: x[44], +[17], ○[46], Δ[31] and ◊47] were superposed after the descriptions

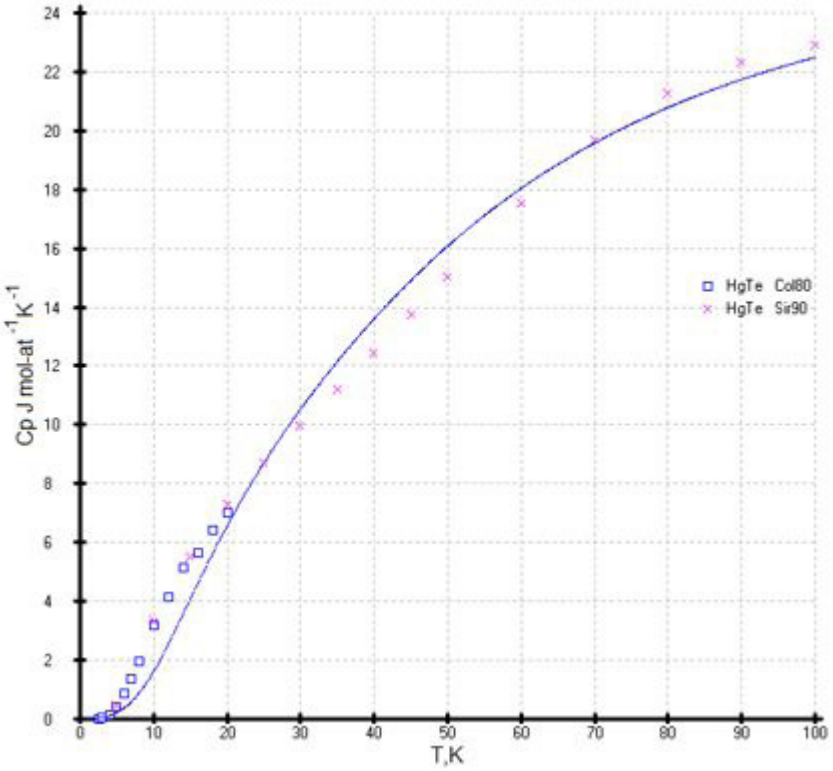

Figure 9: The optimized curve Cp(T) for HgTe using a combination of this model and multiparameter family of functions [10] and the superposed experimental points ❐[45] and x[47]

The low temperature data [45] and [47] below 20K (Fig.9) were not used since these results are overestimated either by the presence of excess tellurium or mercury, or by the presence of impurities. These data represent in the unusual bend of the curve $C_p(T)$ in relation to our calculations.

HgS and diamond-like Pb phases

There are no published available data on the heat capacity of the HgS and diamond-like Pb phases, but our model gives the possibility to calculate these values. They are presented in Tables 3 and 4 and Fig.11 and 12. The virtual heat capacity of the flerovium element (^{114}Fl), belonging to the fourth group of the Periodic system, has a heat capacity of 30.5±0.3 J mol-at^{-1} K^{-1} at temperatures above 3-4K and runs almost parallel to the abscissa axis. At temperatures below 4K, the curve is "pressed" to the ordinate axis. All values of heat capacities above their melting points need to be considered in the metastable solid state. Table 5 represents the calculated ultimate heat capacities with precision up to 1-2% of fluorite phases near their melting point according to ref. [20]. The temperature of the melting points of diamond-like Pb and (^{114}Fl) are not known.

Table 5: Maximal temperature of the existence of sphalerite phases and their ultimate C_p (J·(mole-at)$^{-1}$·K^{-1}) in solid state [20]

Phase	Si	AlP	AlAs	GaP	Ge	InP	α-Sn T_{tr}	InSb	CdTe	HgS	HgSe	HgTe	Pb
T_mK	1688 ±3	2800 ±50	2013 ±20	1790 ±20	1210.3 ±0.5	1344 ±1	287.15 ±1	795.35 ±0.3	1269 ±3	1098 ±5	1072 ±5	943 ±5	600.58 ±0.1
C_p	27.90	30.03	28.57	28.14	28.46	29.06	24.91	27.57	29.40	28.67	28.91	28.87	28.76

The general trend of the heat capacities of sphalerites phases in the region of high and low temperatures are shown in Figure 10 and Figure 11

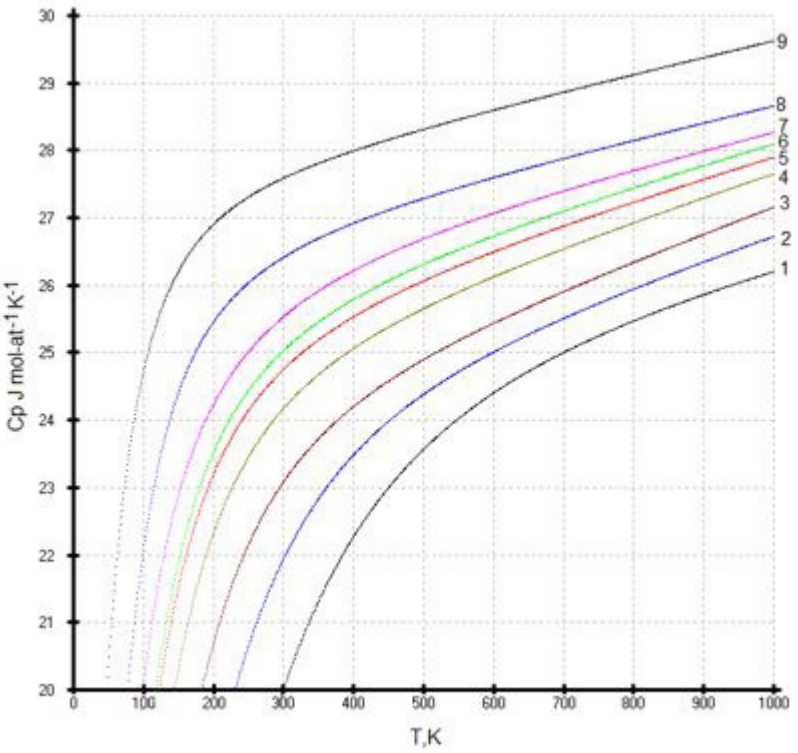

Figure 10: The heat capacities of diamond-like phases at the region of temperature 0-1000K. 9- Pb, 8-HgTe, 7- HgSe, 6-α-Sn (green), 5-HgS (red), 4-GaSb, 3-Ge, 2- GaP, 1-Si; The $C_p(T)$ of diamond-like phases are localized at the point C_p = 30.5 J mol-at^{-1} K^{-1}= 3.67 R or Ln (C_p/R) = 1.3 for Ln (^{114}Fl) = 4.7362 [9]

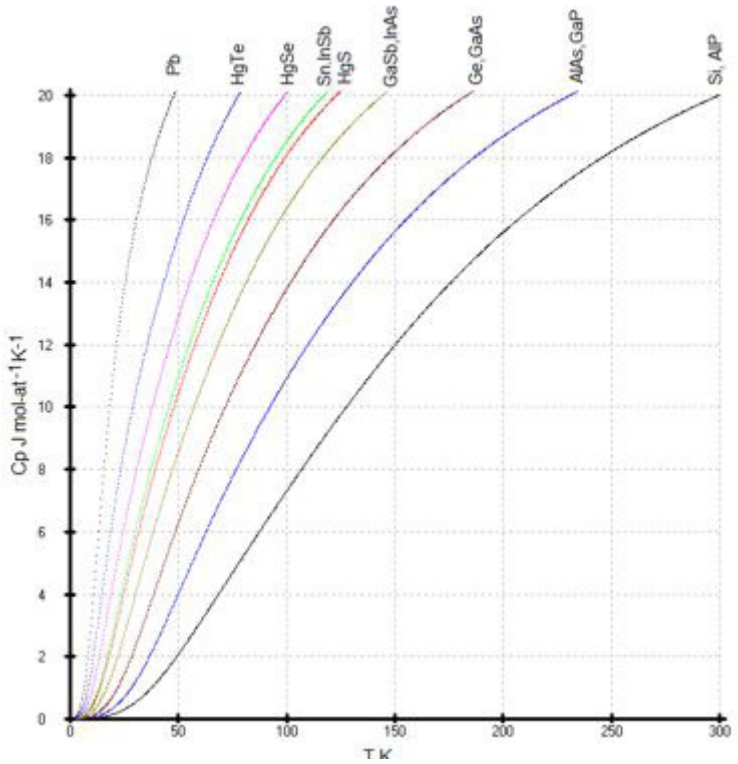

Figure 11: The low temperature heat capacities of diamond-like phases at the region of temperature 0-300K

Summing up the results of this work, it is appropriate to cite a recent article on the influence of intrinsic plane defects of a crystal on the high-temperature specific heat [48]. Authors [48] state: "High temperature specific heat in solids was found to deviate from the '3R' constant, prescribed by the phonon theory of solids and the Dulong-Petit law. Common consent seems to be that anharmonicity effects in phonon vibration are culpable of this, but their effect is usually small and can't fully explain the deviation of high-temperature specific heat, which can reach an 3R-value". The Dulong-Petit law has been used as a postulate since 1818, although it has not been tested and, in fact, cannot be tested. We fully agree with the author's' statement [48], provided that we are talking about an ideal crystal that does not have any foreign inclusions, defects, or dislocations. If we are talking about a non-ideal crystal, then the deviation will be greater than 3R.

Gusev in his recent work [49] uses the so-called "universal scaling" in his concept, which is essentially a similarity method, but this concept can only be applied in the low-temperature region.

Conclusion

1. An unconventional approach was used to optimize the heat capacities of isostructural diamond-like phases as a single system using the multiparameter family of functions [10]. The uncertainty in the extrapolation of $C_p(T)$ at high temperatures is eliminated due to the tight binding of the heat capacity values to one point.

2. The Maier-Kellye equation is quite suitable for describing the heat capacity of the high-temperature region from 250-T_mK.

3. One of the main advantages of the presented work is the method for determining the reference point of the high-temperature heat capacity based on the low-temperature heat capacity and its application to various classes of isostructural compounds.

4. A convenient method has been found for describing low-temperature heat capacities, which makes it possible to avoid measurement errors associated with deviations from stoichiometry, crystal structural defects, and impurities.

5. By using an unconventional approach, we were able to optimize the heat capacities of the sphalerite phases in the solid state. Therefore, the extension of this study to other isostructural phases seems possible and promising.

6. The main rule for a set of isostructural phases is the absence of intersections of the heat capacity curves $C_p(T)$ with each other.

7. Thus, the heat capacities $C_p(T)$ for diamond-like phases with a sphalerite structure were revised in accordance with this new concept. A new description of the heat capacity of gray tin is proposed in accordance with the analysis of the entire class of sphalerite diamond-like phases: Si and AlP, Ge and GaAs, GaP and AlAs, GaAsb and InAs, gray tin and InSb, as well as CdTe, HgS, HgSe, HgTe and Pb.

8. The calculated heat capacities $C_p(T)$ of sphalerite structure are recommended for placement in the hand books. Such data allow one to optimize the thermal conditions of crystal growth and perform calculations necessary for vapor phase epitaxy. They are also necessary for the development of the theory of solid state physics.

Acknowledgements

I would like to thank J.-C. Gachon, Prof. of Physics, (Henry Poincare University (Nancy 1, France); J.P. Bros, Prof. of Chemistry, (Polytechnic University, Marseille, France), S.A. Leonov, Prof. of Mathematics (National Nuclear Research University, Moscow, Russia), Alex Taldrik, PhD in Chemistry (Institute of Superconductivity and Solid State Physics, Moscow, Russia) for the useful discussion, and Prof. Lorie Wood from the University of Colorado (USA) for the language help.

Funding

This work was financially supported by the Russian Foundation for Basic Research (project no. 19-08-01723).

References

1. Petit AT, Dulong PL (1819) Recherches sur quelques points importants de la théorie de la chaleur Annales de chimie et de physique 10: 395-413

2. D Zou, Sh Xie, Y Liu, J Lin, J Li First-principles study of thermoelectric and lattice vibrational properties of chalcopyrite CuGaTe2 J Alloys Comp 570 (2013) 150-155 https://doio-rg/101016/jjallcom201303174

3. Wang H, Jin G, Tan Q (2020) Thermal expansion and specific heat capacity of wurtzite AlN 2020 3rd International Conference on Electron Device and Mechanical Engineering (ICEDME)

4. Vassiliev VP, Gong WP, Taldrik AF, Kulinich SA (2013) Method of the correlative optimization of heat capacities of isostructural compounds J Alloys and Comp 552: 248-254

5. Krygier A, Powell PD, McNaney JM, Huntington CM, Prisbrey ST, Remington BA, et al (2019) Extreme Hardening of Pb at High Pressure and Strain Rate Phys Review Letters 123: 205701

6. Sommerfeld Zur A (1916) Quantentheorie der Spektrallinien. Annal Physik 356: 1-4.

7. Garrone E, Areán CO, Bonelli B (2017) How Many Chemical Elements are there in the Universe? A (not so) Bohring Question. World Journal of Chemical Education 5: 20-22.

8. Ts Y (2020) Oganessian Periodic Table after 150 years. Bulletin of the Russian Academy of Science 90 207-213.

9. Vassiliev VP (2021) Optimization of the Heat Capacities of Diamond-Like Compounds. J Materials Science and Eng B 11: 76-80.

10. Vassiliev VP, Taldrik AF (2021) Description of the heat capacity of solid phases by a multiparameter family of functions 872:159682.

11. Desnoyers JE, Morrison JA (1958) The heat capacity of diamond between 12·8° and 277°K The Philosophical Magazine: J Theor Exp Appl Phys 3: 42-48.

12. Victor AC (1962) Heat Capacity of Diamond at High Temperatures. J Chem Physics 36: 1903-1911.

13. Vasil'ev OO, Muratov VB, Duda TI (2010) The Study of Low Temperature Heat Capacity of Diamond: Calculation and Experiment. J Superhard Materials 32: 375-382.

14. Estermann I, Weertman JR (1952) Specific Heat of Germanium between 20°K and 200°K. J Chem Phys 20: 972.

15. Devyatykh GG, Gusev AV, Gibin AM, Timofeev OV (1997) Heat capacity of high-purity silicon. Russian Inorg Materials 33: 1206-1209.

16. Timofeev OV (1999) The Heat Capacity of High-Purity Silicon, PhD Specialty 020019 Nizhny Novgorod, 1999, 199 P, O V Timofeyev, Teployemkost' vysokochistogo kremniya, Kand Diss Spetsial'nost' 020019 Nizhniy Novgorod 199.

17. Gambino M, Vassiliev V, Bros JP (1991) Molar heat capacities of CdTe, HgTe and CdTe-HgTe alloys in the solid state. J Alloys Comp 176: 13-24.

18. Endo RK, Fujihara Y, Susa M (2006) Calculation of the heat capacity of silicon by molecular dynamic simulation. High Temperature-High Pressure 36: 505-511.

19. Liang SM, Schmid-Fetzer R (2013) Thermodynamic assessment of the Al–P system based on original experimental data, CALPHAD: 42: 76-85.

20. Electronic handbook: Thermodynamic Constance of Substances http://wwwchemmsusu/cgi-bin/tkvpl?show=welcomehtml

21. Desai PD (1986) Thermodynamic properties of Iron and Silicon. J Phys Chem Ref Data 15: 967-983.

22. Wright JT, Carbaugh DJ, Haggerty ME, Richard AL, Ingram DC, et al. (2016) Thermal oxidation of silicon in a residual oxygen atmosphere the RESOX process for self-limiting growth of thin silicon dioxide films. Semicond Sci Technol 31: 105007.

23. Flubacher P, Leadbetter AJ, Morrison JA (1959) The heat capacity of pure silicon and germanium and properties of their vibrational frequency spectra, Philosoph Magazine 39: 273-294.

24. Piesbergen U (1963) Die durchschnittlichen Atomwärmen der AIIIBV Halbleiter AlSb, GaAs, GaSb, InP, InAs, InSb und die Atomwarme des Elements Ge zwischen 12-273 K Naturwissenschaften l8a: 141 -147.

25. Hill RW, Parkinson DH (1952) XXV The specific heats of germanium and grey tin at low temperatures, The London, Edinburgh, and Dublin Phil. Magazine and J Science 43: 309-316.

26. Leadbetter AJ, Settatree GR (1969) Anharmonic effects in the thermodynamic properties of solids VI Germanium: heat capacity between 30 and 500 °C and analysis of data. J Phys C: Solid State Phys 2: 1105-1112. 27. Wagman DD, Evans WH, Parker VB, et al. (1965) Nat Bur Standards Techn Note 270-1. Washington.

28. Tarassov VV and Demidenko BF (1968) Heat capacity and quasi-chain dynamics of diamond-like structure. Phys Status Solidi B 30: 147.

29. Irwin JC, Lacomb J (1974) Specific heats of ZnTe, ZnSe, and GaP. Appl Phys 45: 567.

30. AF Demidenko, VI Koschenko, AS Pashinkin, VE Yachmenev (1981) Low-temperature heat capacity of gallium phosphide. Russ Inorg Mater 17: 677.

31. Pankratz LB (1965) Bureau of Mines (USA), Report of Investigations 6592.

32. Pässler R (2013) Non-Debye heat capacity formula refined and applied to GaP, GaAs, GaSb, InP, InAs, and InSb AIP Advances 3: 082108.

33. Lichter BD, Sommelet P (1969) Thermal Properties of AIIIBV Compounds I High-Temperature Heat Constants and heat Fusion of InSb, GaSb, and AlSb. Trans Met 245: 99-105.

34. Glazov VM and Pashinkin AS (2000) Thermal Expansion and Heat Capacity of GaAs and InAs, Inorg Materials 36 225-231.

35. Pashinkin AS, Fedorov VA, Malkova AS (2010) Heat capacity of GaBV and InBV (BV = P, As, Sb) above 298 K. Inorg Mater 46: 1007-1012.

36. Brönsted JN (1914) Studien zur chemischen Affinität, IX Die allotrope Zinn Umwandlung. Z Phys Chem 88U: 479-489.

37. Webb FJ, Wilks J (1955) The measurement of lattice specific heats at low temperatures using a heat switch. Proc Roy Soc 230: 549-559.

38. Lange F (1924) Untersuchungen uber die spezifische Warme bei tiefen Temperaturen. Z Phys Chem Leipz 110: 343-362.

39. Hultgren R, et al. (1973) Selected Values of the Thermodynamic Properties of the Elements, American Society for Metals, Metals Park, Ohio.

40. Zeng G, McDonald SD, Gu Q, Matsumura S, Nogita K (2015) Kinetics of the β → α Transformation of Tin: Role of α-Tin Nucleation. Cryst Growth Des 15: 5767-5773.

41. Khvan AV, Babkina T, Dinsdale AT, Uspenskaya IA, Fartushina IV, et al. (2019) Thermodynamic properties of tin: Part I Experimental investigation, abinitio modelling of α-, β-phase and a thermodynamic description for pure metal in solid and liquid state from 0 K, CALPHAD 65: 50-72.

42. Styrkas AD (2003) Growth of Gray Tin Crystals. Inorg Materials 39: 683-686. Translated Neorg Materialy 39: 808-811.

43. Styrkas AD (2005) Preparation of Shaped Gray Tin Crystals. Inorg Materials 41: 580-584 Translated Neorg. Materialy 41: 671-675.

44. Cardona M, Kremer RK, Lauck R, Siegle G, Muñoz A, and Romero AH (2009) Electronic, vibrational, and thermodynamic properties of metacinnabar β-HgS, HgSe, and HgTe. Phys Rev B 80: 195204.

45. Collins JG, White GK, Birch JA, Smith TF (1980) Thermal expansion of ZnTe and HgTe and heat capacity of HgTe at low temperatures J Physics C: Solid State Phys 13: 01649-1656.

46. Kelemen F, Cruceanu E, Miculescu D (1965) Phys State Solidi 11: 865- 872.

47. Sirota NN, Gavaleshko PP, Novikova VV, Novikov AV, Frassunyak VM (1990) Heat capacity and thermodynamic functions of solid solutions (CdTe) x (HgTe) 1-x in the range of 5-300K. Russ J Phys Chemistry 64: 1126-1130.

48. Kondrin MV, Lebed YB, Brazhkin VV (2021) Intrinsic planar defects in germanium and their contribution to the excess specific heat at high temperatures. Phys Stat Solidi 1-8.

49. Gusev YV (2021) Experimental verification of the field theory of specific heat with the scaling in crystalline matter. Sci Rep 11: 18155.